Plasma Sprayed Hydroxyapatite Coatings: Understanding Process Relationships using Design of Experiment Analysis

Tanya J. Levingstone [1,2,3,4], Malika Ardhaoui[5], Khaled Benyounis[1,2,3], Lisa Looney [1,2,3], Joseph T. Stokes [1,2,3]

[1]National Centre for Plasma Science and Technology, Dublin City University, Dublin Ireland

[2]Centre for Medical Engineering Research, Dublin City University, Dublin Ireland

[3] School of Mechanical and Manufacturing Engineering, Dublin City University, Dublin 9, Ireland.

[4]Tissue Engineering Research Group, Dept. of Anatomy, Royal College of Surgeons in Ireland, 123 St. Stephen's Green, Dublin 2, Ireland.

[5]Surface Engineering Research Group, School of Electrical, Electronic and Mechanical Engineering, University College Dublin, Belfield, Dublin 4, Ireland.

Corresponding Author:

Dr. Tanya Levingstone

Tissue Engineering Research Group,

Dept. of Anatomy, Royal College of Surgeons in Ireland,

123 St. Stephen's Green,

Dublin 2, Ireland.

tanyalevingstone@rcsi.ie

Abstract

The biocompatibility and osteoconductivity of hydroxyapatite (HA) coatings have led to their use in a wide range of applications in dentistry and orthopaedics. One such application is for the uncemented fixation of implants, where coatings are commonly applied to titanium implants using a plasma thermal spraying process. The spraying process is affected by a large number of parameters leading to highly complex process – property – structure relationships. In a step forward from one-at-a-time analyses, this study used Design of Experiment (DOE) methodology to investigate the simultaneous effects of key plasma spray process parameters on hydroxyapatite coatings for biomedical applications. The effects of five plasma spray process parameters (current, gas flow rate, powder feed rate, spray distance and carrier gas flow rate) on the roughness, crystallinity and purity of hydroxyapatite coatings was determined using a fractional factorial design. The results of this study enabled identification of consistent and competing influences within the process and the identification of some first order interactions. In particular, the diffuse particle size of the HA feedstock powder was found to influence the responses observed within the parameter range investigated. The roughness of HA coatings was found to relate to the particle velocity and the degree of particle melting occurring, withhigher coating roughness resulting when current was high, gas flow rate was low and powder feed rate was high. Highest coating crystallinity resulted at high current, low spray distance and low carrier gas flow rate. Under these conditions deposition of larger HA particles resulted leading to higher amounts of bulk crystalline material and the low spray distance increased the substrate temperature allowing amorphous material to recrystallise. Coating purity relates directly to thermal decomposition of the particles within the plasma jet with a high purity

coating resulting at low particle temperatures i.e at the lower ranges of powder feed rate, spray distance and carrier gas flow rate. This study thus brings greater clarity on the effects of plasma spray process parameters on the properties of resultant hydroxyapatite coatings.

Keywords

Plasma spraying, hydroxyapatite, Design of Experiment (DOE)

1. Introduction

Hydroxyapatite (HA; $Ca_{10}(PO_4)_6(OH)_2$) is a bioceramic with a composition similar to that of the mineral component of bone. It is biocompatible and osteoconductive, allowing the growth on bone cells on its surface [1, 2, 3, 4, 5]. As a result of its favourable biological properties it has been used successfully for many applications in dentistry and orthopaedics. One such application is as a coating applied to hip implants, where it provides implant fixation. The most commonly used method for the production of HA coatings is the atmospheric plasma spraying (APS) process [6, 7]. This is a thermal spray process in which powder particles are melted in a plasma jet and propelled towards the substrate material. The process involves passing a readily ionised gas through an electric arc, formed between a cathode and an anode, resulting in the formation of a plasma jet. The plasma formed is unstable and quickly recombines releasing a large amount of thermal energy. Particles are fed into this high temperature jet, melted and propelled at high velocities towards the substrate. Temperatures involved can potentially be in excess of 15,000°C depending on the selected process parameters [8,9,10]. The process has been used for many

years to apply of a variety of coatings used to protect surfaces from severe harsh environments, such as, wear, corrosion and thermal effects.

Atmospheric (air) plasma spraying (APS) is a complicated process, affected by as many as 50 parameters, and for this reason the process - property – structure relationship are still not fully understood [11,12]. Clinically, HA coated implants have been found to remain functional *in vivo* for up to 15 years [13]. HA coatings are naturally resorbed in the body, releasing calcium and phosphorus ions needed to enable replacement of the coating by ingrowing bone tissue over time; however, delamination or rapid dissolution due to coating instability can lead to short-term implant failure [2, 14,15]. The stability of HA coatings has been shown to be largely affected by its crystallinity and purity [3]. Highly amorphous coatings dissolve more quickly leading to the rapid weakening and disintegration of the coating [3,16]. Coatings with a high degree of crystallinity have lower dissolution rates and are thus more stable *in vivo* [11]. The production of HA coatings using APS has added complexities relating to the decomposition of HA at high temperatures leading to the formation of less stable calcium phosphate phases, such as α-tricalcium phosphate (α-TCP), β-tricalcium phosphate (β-TCP), tetracalcium phosphate (TTCP) and calcium oxide (CaO) [17-20]. Control over the phase purity of HA coatings is thus critically important. In terms of requirements for biomedical applications, ISO standards for hydroxyapatite coatings specify a requirement for a crystallinity of > 45 % and a purity of > 95 % [21]. In addition, early biological responses to HA coatings are influenced by the surface roughness of the coating which affects osteoblast cell attachment and thus bone growth on the coating once it is implanted into the body. Whereas fibroblasts and epithelial cells prefer smoother

surfaces, osteoblasts attach and proliferation better on rough surfaces [22, 23]. It is thus clear that in order to improve implant life, the tayloring of the properties of HA coatings is necessary [24, 25]. This can only be achieved through a clearer understanding of the spraying process.

Numerous studies have investigated the effects of varying process parameters on various properties of HA coatings [6, 25-37]. Contradictions exist within the literature, for example, increased power or current was found by Tsui *et al*. [30] and Sun *et al*. [28] to lead to a decrease in the purity and crystallinity of HA coatings. However, Yang *et al.* [31] found crystallinity to increase with increasing spray current. Dyshlovenko *et al*. [38-39] and Cizek and Khor [40] report net power to have the greatest influence on crystallinity. One method that has been successfully used in order to establish the relationship between process parameters and the properties of a resultant coating is the Design of Experiment (DOE) technique. DOE studies of a variety of plasma sprayed coatings have been carried out, including alumina [11, 41], titanium dioxide [42, 43], zirconia [44, 45], titanium nitride [46] and alumina-titania [11, 47]. DOE experimental techniques have also been applied in the investigation of the complex process relationships involved in plasma sprayed hydroxyapatite coatings [39-40, 48-53]. While these studies have brought about some clarity to the relationships between the spray process parameters and resultant HA coating properties, further understanding of these relationships is required. In this study, a Design of Experiment (DOE) methodology has been used in order to gain additional understanding of parameter interaction and desirable parameter ranges for plasma spraying of HA coatings. The specific objectives of the study were to assess the effects of varying five

process parameters: current (A), gas flow rate (B), powder feed rate (C), spray distance (D) and carrier gas flow rate (E), on the crystallinity, purity and roughness of plasma sprayed hydroxyapatite coatings; key properties that influence coating stability and cellular response upon implantation.

2. Experimental Methods

2.1. Materials

Titanium alloy, Ti6Al4V, was selected as the substrate material in this study as it is typically used in femoral implants as the receiving substrate for HA coatings. Discs, 10 mm in diameter with a thickness of 2 mm, were used. The discs were grit-blasted prior to spraying at a pressure of 5 bars and an angle of incidence of 75°, using pure white aluminium oxide (Al_2O_3) grit with a particle size of 500 µm (mesh 36), selected due to its biocompatibility. After grit blasting, loose grit particles were removed using high pressure air. The discs were then cleaned for 5 mins in an ultrasonic cleaner. The average surface roughness (Ra) of the discs was determined, using the Surftest 402 surface profilometer, to be approximately 3.2 µm.

The HA powder used for the coating process was Captal 60-1 Thermal Spraying HA powder (Plasma Biotal Ltd, UK). This powder is reported by the manufacturer to have an average particle size of 45 µm. Particle size analysis was carried out using the Malvern Mastersizer particle size analyser to determine the particle size distribution. Powder morphology was examined using scanning electron microscopy (SEM) (LEO 440 Stereo Scan, Leica, UK), using a current of 150 pA, accelerating voltage of 15 KeV and a

138 magnification range of 50-200 x. The surface area of the powder was determined using
139 Micromeritics GEMINI BET surface area analyser (Georgia, USA). Powder particle
140 density was determined using the Helium Pycnometer (Micromeritics, Georgia, USA).
141

142 2.2. Experimental Design

143 The experiment was designed using the statistical software, Design-Expert 7.0 (Stat-Ease
144 Inc., Minneapolis, USA). A ¼ fraction fractional factorial design (2^{5-2} design) was used to
145 investigate the effect of various process parameters (factors) on the properties of HA
146 coatings. Five factors were investigated, current (A), gas flow rate (B), powder feed rate
147 (C), spray distance (D) and carrier gas flow rate (E). Two levels were selected for each
148 parameter, based on parameters levels that are currently reported in literature (N1-N8) [26-
149 31, 39, 50, 54]. In addition, three centre point experiments were included to provide a
150 measure of process stability and inherent variability while also checking for curvature (N9-
151 N11). The parameter ranges selected are detailed in Table 1. The design consisted of 11
152 experiments, details of which are given in Table 2. The experiments were carried out in
153 random order to ensure that systematic errors did not influence the results.
154

155 A polynomial equation was used to describe the relationship between the experimental
156 factors and each response (Equation 1):
157

158 $$Y = \beta_0 + \sum_{i=1}^{5} \beta_i X_i$$ .....[Eqn. 1]

159

where Y is the response, β_0 is the mean value of the response, βi represents the coefficient of the variable Xi.

The results obtained from the study were analysed using the Design Expert software. The main affects on each response were modelled using the backward selection method to elimate insignificant terms (P-value ≤ 0.01). The analysis of variance (ANOVA) test was used to determine the statistical significance of the developed equations. Statistical measures, R^2, Adjusted R^2, Predicted R^2 and Adequate Precision, were used to determine the adequacy of the resultant equations. The most important of these measures is the R^2 value, which is a number between 0 and 1 and should be greater than 0.6 in order to indicate an adequate equation [55].

2.3. Plasma Spraying

Plasma thermal spraying was carried out using a Sulzer Metco 9MB plasmatronfitted with a 3M7-GH nozzle (Sulzer Metco, Winterthur, Switzerland). High purity argon was used as both the plasma forming gas and the powder carrier gas. No secondary gas was used. A traverse speed of 38 mm/s and a spray time of 35 s were used for all coatings, resulting in 15 passes of the spray gun. Coatings were sprayed according to the experimental matrix described in Table 2.

2.4. Coating Characterisation

Three responses were measured, roughness, crystallinity, and purity. Surface roughness, Ra, was measured using the Surftest 402 surface profilometer (Mitutoyo, Michigan, US). Four measurements were taken for each sample, with the sample orientation changed between each measurement. The surface morphology of each coating was also examined using the LEO 440 Stereo Scan Scanning Electron Microscope, using a current of 150 pA, accelerating voltage of 15 KeV and a magnification range of 50-200 x. The crystallinity and purity of HA coatings were determined from X-ray diffraction patterns, obtained using the Bruker D-8 Advance Diffractometer (Coventry, UK) with a copper anode. A locked-couple scan was carried out between 20 and 60º 2θ. An increment of 0.02 and a scan speed of 5 sec/step were applied.

The % crystallinity was calculated by comparing the crystalline area of the XRD pattern to the total XRD pattern area, using Equation 2 [28, 30, 56, 57]. The % purity was calculated by comparing the impurity area to the total crystalline area, using Equation 3. The areas used for the crystallinity and purity calculations were identified and measured using the curve fitting function in the Bruker Diffract Plus EVA software (Bruker AXS, UK). Crystallinity and purity measurements were repeated three times for each coating.

$$Crystallinity(\%) = \frac{A_C}{A_T} x100 \quad \text{.....[Eqn. 2]}$$

where A_T is the area under the total diffraction pattern and A_C is area under the diffraction pattern once the amorphous part of the pattern has been removed using the curve fitting function in the Bruker Diffract Plus EVA software (Bruker AXS, UK)..

$$Purity(\%) = \frac{A_I}{A_C} x100 \quad \text{.....[Eqn. 3]}$$

where A_C is the crystalline area from the diffraction pattern and A_I is the total impurity area, i.e. the sum of the areas of the peaks between 29º 2θ and the base of the tallest HA peak (2 1 1 peak).

3. Results

3.1. Powder Characterisation

The initial HA powder was found to have an irregular morphology, as can be seen from the micrograph in Fig. 1. The particle size analysis results, shown in Fig. 2, indicate that the size of the particles fall within two separate clusters, one between 0.1 and 1.0 μm and the other between 10 and 100 μm. The mean particle size of the HA powder was found, from the laser particle size analysis, to be 38.3 μm. The average density of the powder sample was found using helium pycnometry to be 3.28 g/cm^3. The surface area of the powder was found using BET surface area analysis to be 0.4640 m^2/g. The HA powder had a crystallinity of 99.96 %. From analysis of the XRD pattern the powder contained 99 % pure HA (JCPDS 9-0432) with a trace amount of tetracalcium phosphate (TTCP, JCPDS 25-1137).

223

224 3.2. Measured Responses

225 Following spraying, each of the resultant coatings was inspected. The measured responses
226 for each experimental run (N1 – N11) are given in Table 3. The coating from run N1 was
227 very thin, with the substrate visible through the coating and thus crystallinity and purity
228 measurements for this sample could not be obtained. In addition, the measured roughness
229 values were very low and were not included in the analysis. The crystallinity and purity
230 measurements for coating N10 were much lower than those of all other coatings and it was
231 thus deemed to be an outlier and was not included in the analysis. The centre point
232 experiments (N9 and N11) showed good process reliability. The surface roughness (Ra) of
233 the coatings was found to vary between 6.2 ± 0.7 μm (N3) and 13.4 ± 0.7 μm (N6).
234 Micrographs of the coatings with the lowest (N3) and highest (N6) Roughness are shown
235 in Fig. 3. The % crystallinity ranged from 65.2 % (N5) to 87.6 % (N2). The XRD patterns
236 for coatings with the lowest (N5) and highest (N2) crystallinity are shown in Figure 4.
237 Micrographs of coatings N5 and N2 are shown in Figure 5 (a) and (b) respectively. The %
238 purity was found to range between 95.5 % (N8) and 99.4 % (N2). The XRD patterns for
239 the coatings with the lowest (N8) and highest (N2) purity are shown in Fig. 6. Overall, all
240 coatings met the > 45 % crystallinity and > 95 % purity required by ISO 13779-2:2000
241 (Implants for surgery- Hydroxyapatite. Coatings of hydroxyapatite) [21].

242

3.3. Roughness

Roughness was found to be significantly affected by three factors: current (A), gas flow rate (B) and powder feed rate (C) (P-value ≤ 0.01), with highest roughness resulting at high current, low gas flow rate and high powder feed rate. The regression equation for roughness is presented in Table 4, expressed in terms of coded factors in Equation 4 and actual factors in Equation 5. The coded factors equation uses the coded low and high levels (-1 and 1) from the experimental design, whereas the actual equation incorporates the numerical differences between the factors in the equation. It can be seen from the coded factors equation (Equation 4), that current has the greatest affect on roughness, followed by gas flow rate and powder feed rate. The predicted vs. actual graph (Fig. 7a), shows that the actual experimental values closely fits the values predicted by the equation, represented as a straight line in the graph. The statistical measures, summarised in Table 5, indicate the a good fit of the data to the equation.

3.4. Crystallinity

Statistical analysis of the results showed that the crystallinity of the coating was significantly affected by the current (A), spray distance (D) and carrier gas flow rate (E) (P-value $\leq$ 0.01). The regression equation for crystallinity is presented in Table 4, expressed in terms of coded factors in Equation 6 and actual factors in Equation 7. Current was found to have the greatest effect, followed by carrier gas flow rate and then spray distance, with highest crystallinity at high current, low spray distance and low carrier gas

flow rate. The statistical measures summarised in Table 5 and predicted vs. actual graph for crystallinity, (Fig. 7 b), indicate a good fit of the data to the equation.

3.5. Purity

Statistical analysis of the results showed that the purity of the coating was significantly affected by the powder feed rate, spray distance and carrier gas flow rate (P-value ≤ 0.01). The regression equation for purity is presented in Table 4, expressed in terms of coded factors in Equation 8 and actual factors in Equation 9. Powder feed rate was found to have the greatest effect, followed by spray distance and carrier gas flow rate, with the highest purity reported at low powder feed rate, low spray distance and low carrier gas flow rate. The statistical measures summarised in Table 5 and predicted vs. actual graph for crystallinity, (Fig. 7 c), indicate a good fit of the data to the equation.

4. Discussion

The plasma thermal spraying process is affected by a large number of parameters including current, gas flow rate, powder feed rate, spray distance and carrier gas flow rate. While there are a range of factors influencing the process, on a mechanistics level, each of these parameters ultimately influence two key aspects; the degree of particle melting within the plasma jet and the velocity at which particles impact the substrate surface. Thus the

influence that each process parameter has on particle melting and particle velocity ultimately determines the properties of the coatings produced. The plasma sprayed coatings produced at the parameter ranges investigated in this study resulted in coatings with widely varying roughness, purity and crystallinity results. Overall, the study showed that while good quality coatings, with suitable roughness, crystallinity and purity values were achieved in experiments N2 to N8, the process settings for experiment N1 did not enable deposition of a coating that fully covered the substrate. Thus, for further studies it is recommended that the parameter range be modified to ensure adequate melting of the particles within the plasma jet.

The roughness of HA coatings produced here ranged between 6.15 μm and 13.4 μm, similar to those reported by Cizek and Khor [40]. Roughness is known to relate to the particle velocity and the degree of particle melting occurring. In this study it was found that high roughness results when the current is high, gas flow rate is low and powder feed rate is high, with the overall effect of these parameters for the high roughness condition leading to increased particle temperature and decreased particle velocity (Table 6). Cizek and Khor reported a similar occurrence with rougher coatings demonstrating individual splat morphologies being formed when particle temperatures were higher [40]. However, these results were contrary to findings reported in other studies [28, 58], where conditions that generally lead to increased particle temperatures were seen to result in lower coating roughness. It was observed from particle size analysis, that the size of the HA particles fall within two separate clusters, one between 0.1 and 1.0 μm and the other between 10 and 100 μm. Thus at the low roughness condition only the smaller powder particles are melted, larger particles remain unmelted and bounce off the surface of the substrate rather than

being deposited onto it. At the high roughness condition all particles are melted and thus the larger particles are incorporated into the coating rather than bouncing off it, resulting in a greater degree of coating roughness. Low particle velocity resulting at the high roughness condition leads to increased dwell time within the plasma and thus allows melting of the larger particles, and the lower velocity at which particles impact the substrate leads to less splat flattening; thus the overall result is a rougher coating. The SEM micrographs (Fig. 3) confirm this, demonstrating a visible difference in the size of the particles present with smaller particles observed in the low roughness coatings (Fig. 3 a) than the high roughness coating (Fig. 3 b). While, the effect of powder feed rate on the temperature and velocity of the plasma flame is known to be minimal [49], higher roughness at higher powder feed rates may be due to greater numbers of overlapping particles and reduced particle spreading.

Coating crystallinity is determined by the degree of particle melting and the particle cooling rate and was found to be highest at high current, low spray distance and low carrier gas flow rate. The crystalline fraction of a HA coating consists of bulk crystalline material resulting from the unmelted central cores of the HA particles and amorphous material that has recrystallised following spraying [28, 60]. The overall expected effects of the high coating crystallinity spraying conditions (N2) are a high coating temperature and low particle cooling rate (Table 7). Thus for this condition, the high current causes an increase in particle melting and an increase in substrate temperature, leading to a low particle cooling rate. The quantity of larger particles deposited at high current is greater, leading to the presence of a greater amount of bulk crystalline material within the coating, leading to

a high % crystallinity. The low spray distance causes particle melting to be low due to reduced residence time in the plasma jet and the substrate temperature to be high as it is closer to the plasma jet, thus leading to a low particle cooling rate which enabled recrystallisation of the amorphous phase. The carrier gas flow rate determines the entry positions of particles into the jet; at low flow rates particles do not enter the center of the plasma jet and thus undergo less melting. This was confirmed by the observed differences in coating splat morphology between the highest crystallinity coating (N2 Fig. 5 a) and the lowest crystallinity coating (N5 Fig. 5 b). The powder particles visible in the low crystallinity coating retain their spherical shape, indicating that only partial melting of the particles occurred, whereas greater particle melting was observed in the high crystallinity coating. Coating crystallinity was found to be reduced significantly compared to the starting HA powder, although all coatings met the >45% crystallinity ISO requirement [21]. The highest coating crystallinity achieved was 87.6% and thus coatings sprayed using these spraying conditions would thus be highly stability *in vivo*.

Coating purity relates directly to thermal decomposition of the particles within the plasma jet with a high purity coating resulting when the spray conditions led to a low particle temperature i.e at the lower ranges of powder feed rate, spray distance and carrier gas flow rate (Table 8). At low powder feed rate, the plasma temperature would be higher than at high powder feed rate, as less cooling of the plasma occurs when fewer particles are injected into it. At low spray distance, the particles only remain in the plasma for a short time and thus experience less heating. At low carrier gas flow rate the particles do not enter the central, hottest part of the plasma jet and thus remain at a lower temperature. While

Cizek and Khor [40] found no distinct relationship between in-flight temperature or velocity and percentage phase change, the findings reported here agree with the finding of Sun *et al.* [28]. Importantly for clinical translation, the purity of all coating was > 95 % as per ISO guidelines [21]. For N2, very low levels of impurity phases were present and a coating purity of 99.4% was achieved.

This study has successfully identified suitable parameter ranges for this spraying process while also investigating the main effects of process parameter on coating roughness, crystallinity and purity. The two-level factorial design employed here provides a valuable tool for identification of the main effects and some first order interactions; however it imposes some constraints and thus presents a limitation in this study. The inclusion of centre point experiments provided a useful addition in demonstrating the stability of the process. Although this study design enabled just linear relationships to be evaluated, assessment of the centre points indicates that there is some curvature in the responses which could be further elucidated through a larger investigation of parameter interactions. In order to understand these responses, further assessment of the plasma spray process is thus currently being undertaken within our lab. The study presented here thus presents and important first step in this investigation. A significant finding in this study is that the degree of powder particle melting that occurs is dependent on the powder particle size distribution of the feedstock powder. The powder used in this study had a large particle size distribution which led to the observation of some unexpected effects. Use of a sieving process may be beneficial in order to reduce the particle size range for future studies. Overall, this study

provides a valuable contribution to the understanding of this complex system and presents predictive process equations for the roughness, crystallinity and purity of plasma sprayed HA coatings, which provide useful tools for coating production and for further development and optimisation of this process.

5. Conclusion

A Design of Experiment study has been used to determine the effects of current, gas flow rate, powder feed rate, spray distance and carrier gas flow rate on the roughness, crystallinity and purity of plasma sprayed hydroxyapatite coatings leading to the identification of consistent and competing influences and first order interactions. The results demonstrated thatcoatings with higher roughness resulted when current was high, gas flow rate was low and powder feed rate was high as under these conditions melting of larger particles occurred enabling them to be deposited in the coating and a lower impact velocity led to less splat flattening. Coating crystallinity was highest at high current, low spray distance and low carrier gas flow rate. Under these conditions deposition of larger HA particles resulted leading to greater amounts of bulk crystalline material and the low spray distance increased the substrate temperature allowing amorphous material to recrystallise. Coating purity related directly to thermal decomposition of the particles within the plasma jet with a high purity coating resulting when the spray conditions led to a low particle temperature i.e at the lower ranges of powder feed rate, spray distance and carrier gas flow rate. These predictive process equations provide a better understanding of

effect of plasma spray properties on the roughness, crystallinity and purity of hydroxyapatite coatings. These findings also demonstrate the effects of a diffuse particle size range on the process showing that increased plasma temperatures are required in order to ensure melting of larger particles. These results thus bring greater clarity on the effects of plasma spray process parameters on the properties of resultant hydroxyapatite coatings and provide the first step in a larger study aimed at further elucidating parameter effects and interactions.

Acknowledgements

The authors would like to acknowledge the research support provided by the Irish Research Council, funded under the National Development Plan.

References

[1] K. Søballe, E. S. Hansen, H. B. Rasmussen, P. H. Jørgensen and C. Bünger, J. Orthopaed. Res., 10, (1992) 285-299.

[2] M. Nagano, T. Nakamura, T. Kokubo, M. Tanahashi and M. Ogawa, Biomaterials, 17 (1996) 1771-1777.

[3] R. B. Heimann, Surf. Coat. Tech., 233 (2013) 27–38.

[4] S. Robbins, C. Lauryssen and M.N. Songer, J. Spinal. Disord. Tech., (2014) Feb 27. [Epub ahead of print]

[5] R.K. Wong, B.M. Gandolfi, H. St-Hilaire, J. Craniofac. Surg. 22 (2011) 1, 247-251.

[6] R. Gadow, A. Killinger, N. Stiegler, Surf. Coat. Tech., 205 (2010) 1157–1164.

[7] R. Surmenev, Surf. Coat. Tech., 206 (2012) 2035-2056.

[8] Oerlikon Metco, [online], www.oerlikon.com/metco, (Accessed 25th June 2015).

[9] M. Roy, A. Bandyopadhyay, S. Bose, Surf. Coat. Tech., 205 (2011) 8, 2785-2792.

[10] R.C, Tucker, ASM Handbook Vol 5A: Thermal Spray Technology, ASM International, Ohio, 2013.

[11] T. J. Steeper, Varacalle, D. J. JR., G. C. Wilson, W. L. Riggs, A. J. Rotolico and J. E. Nerz, J. Therm. Spray. Technol., 2 (1993) 251-256.

[12] G. Singh, S. Singh, S. Prakash, Surf. Coat. Tech., 205 (2011) 20, 4814 – 4820.

[13] Department of Orthopaedic Surgery Haukeland University Hospital, "The Norwegian Arthroplasty Register Report 2010", [online], http://nrlweb.ihelse.net/eng/Report_2010.pdf, (Accessed 9th May 2015)

[14] L. Sun, C. C. Berndt, K. A. Gross and A. Kucuk, J. Biomed. Mater. Res., 58 (2001) 570-592.

[15] F. Fazan and P. M. Marguis, J. Mater. Science: Mater. Med., 11 (2000) 787-792.

[16] G. Bolelli, D. Bellucci, V. Cannillo, L. Lusvarghi, A. Sola, P. Müller, A. Killinger, R. Gadow, L. Altomare, L. De Nardo, N. Stiegler, Mater Sci Eng C, 34 (2014) 287–303.

441 [17] T. M. Sridhar, U. Kamachi Mudali and M. Subbaiyan, Corros. Sci., 45 (2003) 2337-
442 2359.

443 [18] Y. Yang, K. Kim, C. M. Agrawal and J. L. Ong, Biomaterials, 25 (2004) 2927-2932.

444 [19] R. B. Heimann, Surf. Coat. Tech., 201 (2006) 2012-2019.

445 [20] N. Cao, J. Dong and Q. Wang, J. Biomed. Mater. Res. A, 92 (2010), 3, 1019-1027.

446 [21] International Organisation for Standards "Implants for Surgery- Hydroxyapatite. Part
447 2: Coatings of Hydroxyapatite", BS ISO 13779-2:2000, 2000.

448 [22] B. D. Boyan, T. W. Hummert, D. D. Dean and Z. Schwartz, Biomaterials, 17 (1996)
449 137-146.

450 [23] A. Boyde, A. Corsi, R. Quarto, R. Cancedda and P. Bianco, Bone, 24 (1999) 579-589.

451 [24] H. Wang, S. Guan, Y. Wang, Colloids Surf., B, 88 (2011), 1, 254-259.

452 [25] G.A. Fielding, M. Roy, A. Bandyopadhyay, Acta. Biomater., 8 (2012) 8, 3144-3152.

453 [26] P. Cheang and K. A. Khor, J. Mater. Process. Tech., 48 (1995) 429-436.

454 [27] S. W. K. Kweh, K. A. Khor and P. Cheang, Biomaterials, 21 (2000) 1223-1234.

455 [28] L. Sun, C. C. Berndt and C. P. Grey, Mater. Sci. Eng. A, 360 (2003) 70-84.

456 [29] Y. P. Lu, S. T. Li, R. F. Zhu and M. S. Li, Surf. Coat. Tech., 157 (2002) 221-225.

457 [30] Y. C. Tsui, C. Doyle and T. W. Clyne, Biomaterials, 19 (1998) 2015-2029.

[31] C. Y. Yang, B. C. Wang, E. Chang and J. D. Wu, J. Mater. Sci: Mater. Med., 6 (1995) 249-257.

[32] X. Bai, K. More, C.M. Rouleau, Acta. Biomater., 6 (2010), 6, 2264-2273.

[33] H. Podlesak, L. Pawlowski, R. d'Haese, J. Therm. Spray Technol., 19 (2010), 3, 657-664.

[34] I. Demnati, M. Parco, D. Grossin, Surf. Coat. Tech., 206 (2012) 8, 2346-2353.

[35] U. Ripamonti, L.C. Roden, L.F. Renton, Biomaterials, 33 (2012) 15, 3813-3823.

[36] S. Durdu, O.F. Deniz, I. Kutbay, J. Alloy Compd., 551 (2013), 422-429.

[37] A. Cattini, D. Bellucci, A. Sola, Biomaterials, 102 (2014) 3, 551-560

[38] S. Dyshlovenko, L. Pawlowski, P. Roussel, D. Murano and A. Le Maguer, Surf. Coat. Tech., 200 (2006), 3845-3855.

[39] S. Dyshlovenko, C. Pierlot, L. Pawlowski, R. Tomaszek and P. Chagnon, Surf. Coat. Tech., 201 (2006) 2054-2060.

[40] J. Cizek, K. A. Khor, Surf. Coat. Tech., 206 (2012) 2181–2191.

[41] J. R. Mawdsley, Y. J. Su, K. T. Faber and T. F. Bernecki, Mater. Sci. Eng. A, 308 (2001) 189-199.

[42] J.G. Malinka, D.J. Varacalle Jr., W.L. Riggs, Thermal Spray: International Advances in Coating Technology, ASM Int., Materials Park, Ohio, USA, 1992, p. 87.

476 [43] S. Forghani, M. Ghazali, A. Muchtar, Ceram. Int., 39 (2013) 3, 551-560.

477 [44] G. Bertrand, P. Bertrand, P. Roy, C. Rio, R. Mevrel, C. Rio, Surf. Coat. Technol., 202
478 (2008) 1994.

479 [45] B. Lin, M. Jean and J. Chou, Appl. Surf. Sci, 253 6 (2007) 3254-3262.

480 [46] J. F. Li, H. Liao, B. Normand, C. Cordier, G. Maurin, J. Foct and C. Coddet, Surf.
481 Coat. Tech., 176 (2003) 1-13.

482 [47] S. P. Sahu, A. Satapathy, Patnaik A, Mater. Design, 31 (2010) 3, 1165-1173.

483 [48] S. Dyshlovenko, L. Pawlowski, B. Pateyron, I. Smurov, J.H. Harding, Surf. Coat.
484 Tech., 200 (2006) 12-13, 3757–3769.

485 [49] J. Cizek, K. A. Khor and Z. Prochazka, Mater. Sci. Eng: C, 27 2 (2007) 340-344.

486 [50] A. Chebbi and J. Stokes, J. Therm. Spray Technol., 21(2012)719-730.

487 [51] R.B. Heimann, J. Therm. Spray Technol., 19 (2010) 4 765-778.

488 [52] H. Farnoush, J. Aghazadeh Mohandesi, D. Haghshenas Fatmehsari, Ceram. Int., 38
489 (2010) 8, 6753-6767.

490 [53] S.S Kalkarni, Y. Yong, M.J. Rys, J. Manuf. Process., 15 (2013) 4, 666-672.

491 [54] Y. Zhao, A. Shinmi, X. Zhao, P.J. Withers, S. Van Boxel, N. Markocsan, P. Nylen, P.
492 Xiao, Surf. Coat. Tech., 206, (2012) 23, 4922–4929.

493 [55] D. C. Montgomery, G. C. Runger and N. R. Hubble, Engineering Statistics, 2nd ed.,
494 John Wiley & Sons, New York, 2001.

495 [56] M. F. Morks and A. Kobayashi, Appl. Surf. Sci., 253, 17 (2007) 7136-7142.

496 [57] L. Keller and W. A. Dollase, J. Biomed. Mater. Res., 49 (2000) 2, 244–249[58] K. A.
497 Gross and M. Babovic, Biomaterials, 23 (2002) 4731-4737.

498 [59] S. Guessasma, G. Montavon and C. Coddet, Surf. Coat. Tech., 192 (2005) 70-76.

499 [60] W. Tong, J. Chen and X. Zhang, Biomaterials, 16 (1995) 829-832.

500
501
502

Tables

Table 1: Parameter ranges selected for the screening experiment

	Low Level ***(-1)***	***High Level*** ***(+1)***
A - Current *(A)*	450	750
B - Gas flow rate *(slpm/scfh)*	33/70	61.4/130
C - Powder feed rate *(g/min)*	10	20
D - Spray distance *(mm)*	80	120
E - Carrier gas flow rate *(slpm/scfh)*	4.7/10	9.4/20

Table 2: Plasma spray screening experiment variables and experimental plan

Exp Name		***Variables***				
		Current (A) *A*	**Gas flow rate (B)** *Slmp (Scfh)*	**Powder feed rate (C)** *g/min*	**Spray distance (D)** *mm*	**Carrier gas flow fate (E)** *Slmp (Scfh)*
¼ Design $-2^{(5-2)}$ (N1-N8)	N1	450	33 (70)	10	120	9.4 (20)
	N2	750	33 (70)	10	80	4.7 (10)
	N3	450	61.4 (130)	10	80	9.4 (20)
	N4	750	61.4 (130)	10	120	4.7 (10)
	N5	450	33 (70)	20	120	4.7 (10)
	N6	750	33 (70)	20	80	9.4 (20)
	N7	450	61.4 (130)	20	80	4.7 (10)
	N8	750	61.4 (130)	20	120	9.4 (20)
Centre points (N9-N11)	N9	600	47.2 (100)	15	100	7.1 (15)
	N10	600	47.2 (100)	15	100	7.1 (15)
	N11	600	47.2 (100)	15	100	7.1 (15)

Table 3: Average Response Values for Roughness, Crystallinity and Purity

Exp Name	*Average Responses*		
	Roughness	**Crystallinity**	**Purity**
	μm	*%*	*%*
N1	4.1	-	-
N2	10.55	87.6	99.4
N3	6.15	65.2	97.8
N4	8.65	81.3	98.9
N5	10.48	65.2	97.6
N6	13.4	77.4	97.7
N7	7.28	77.8	98.2
N8	11.03	65.8	96.4
N9	10.65	79.9	97.4
N10	9.48	54.9	95.5
N11	10.6	76.1	97.2

528 **Table 4: Coded and actual experimental equations for Roughness, Crystallinity and Purity**

Response	Coded and Actual Regression Equations	Eqn. No.
Roughness	Roughness = + 9.45 + 1.4 * A – 1.17 * B + 1.10 * C	**Eqn. 4**
	Roughness = + 4.257 + 9.70417 E-003 * Current – 0.039146 * Gas flow rate + 0.21912 * Powder feed rate	**Eqn. 5**
Crystallinity	Crystallinity = + 71.83 + 6.2 * A – 5.16 * D – 6.14 * E	**Eqn. 6**
	Crystallinity = + 91.25062 + 0.041329 * Current – 0.25797 * Spray distance – 1.22839* Carrier gas flow rate	**Eqn. 7**
Purity	Purity = + 97.93 – 0.46 * C – 0.34 * D – 0.59 * E	**Eqn. 8**
	Purity = + 102.8 – 0.09125 * Powder feed rate – 0.017187 * Spray distance – 0.11875 * Carrier gas flow rate	**Eqn. 9**

529

530

Table 5: Statistical Measures of Equation Adequacy

Statistical Measure	***Roughness***	***Crystallinity***	***Purity***
R^2	0.95	0.96	0.91
Adjusted R^2	0.92	0.92	0.85
Predicted R^2	0.82	0.81	0.56
Adequate Precision	17.776	14.902	10.44

534 **Table 6: Overall effect on particle temperature and velocity for high roughness spray conditions**

Factor		***Particle Temperature***	***Particle Velocity***
Current	↑	↑	↑
Gas flow rate	↓	↑	↓
Powder feed rate	↑	↓	
Overall effect		↑	↓

535

536

Table 7: Overall effect on plasma temperature and velocity for high crystallinity spray conditions

Factor		*Particle Melting*	*Particle Cooling Rate*
Current	↑	↑	↓
Spray distance	↓	↓	↓
Carrier gas flow rate	↓	↓	
Overall effect		↑	↓

Table 8: Overall effect on particle temperature for high purity spray conditions

Factor		*Particle Temperature*
Powder feed rate	↓	↑
Spray distance	↓	↓
Carrier gas flow rate	↓	↓
Overall effect		↓

Figures Captions

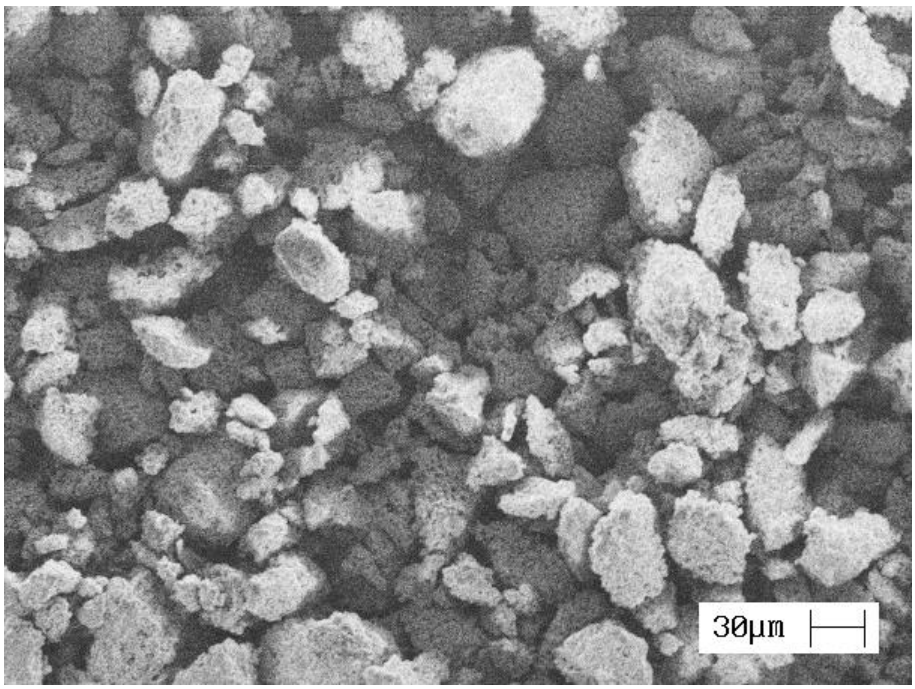

Figure 1: SEM micrograph of Plasma Biotal Captal 60-1 HA Powder

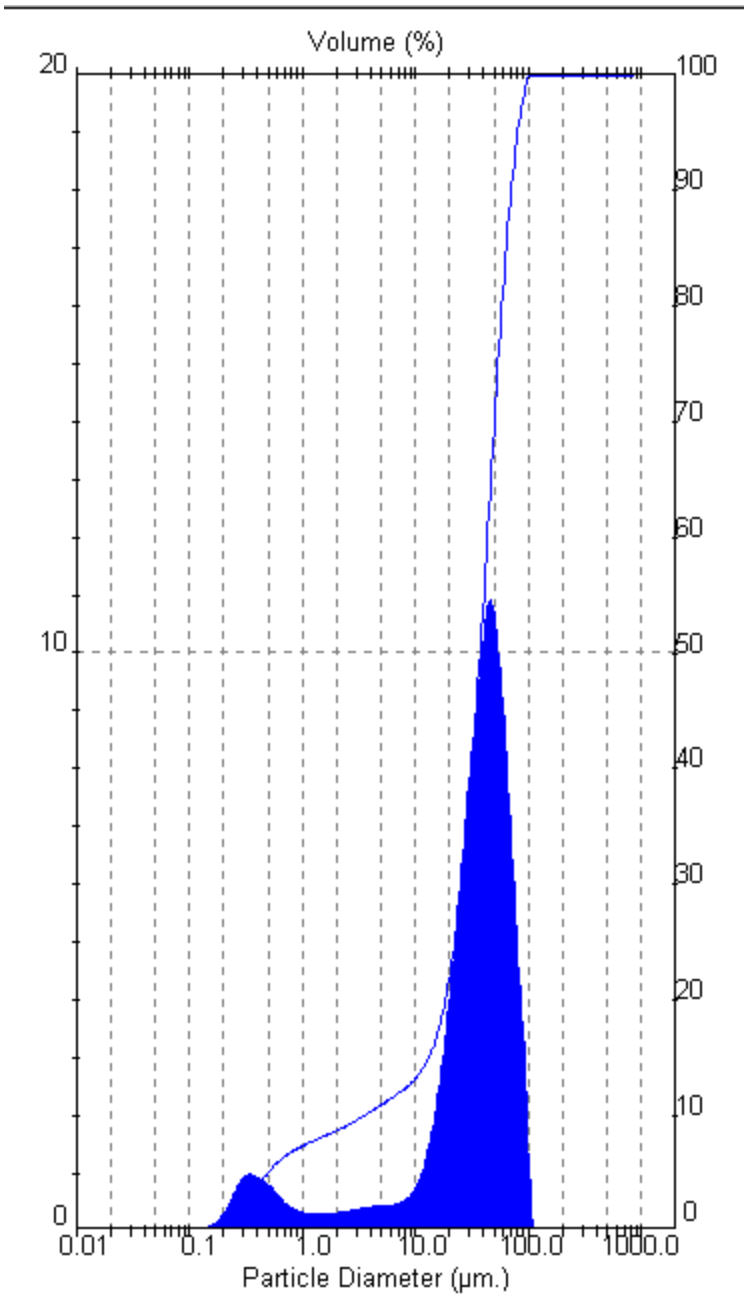

547

548 Figure 2: Particle Size Distribution of Plasma Biotal Captal 60-1 HA Powder. Power
549 particles fall within two separate clusters, one between 0.1 and 1.0 µm and the other
550 between 10 and 100 µm with the mean particle size found to be 38.3 µm.

551

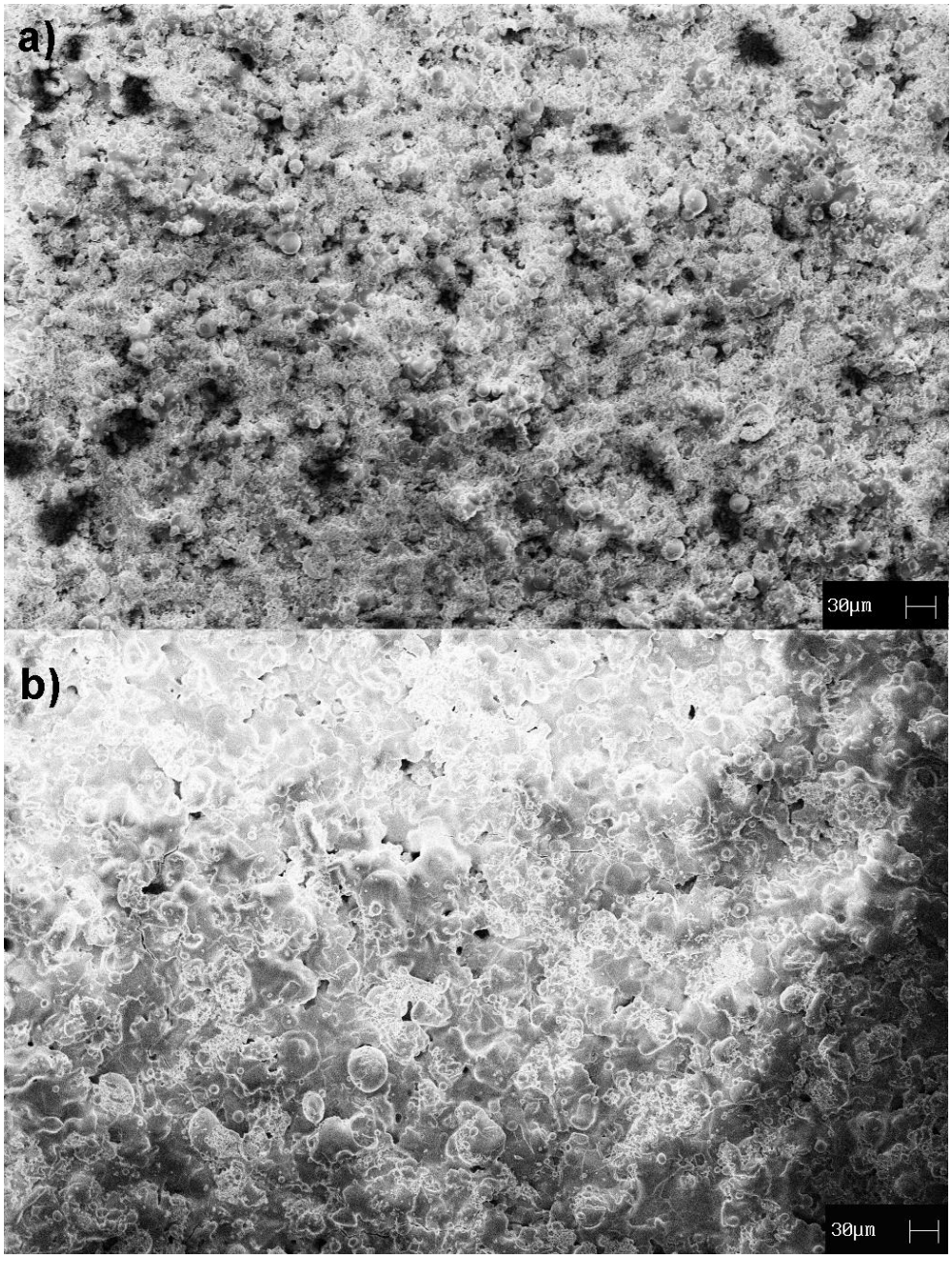

552

553 Figure 3: SEM micrographs showing the surface morphology of a) coating N3 and b) N6.

554 Coating N3 had the lowest roughness and coating N6 had the highest roughness.

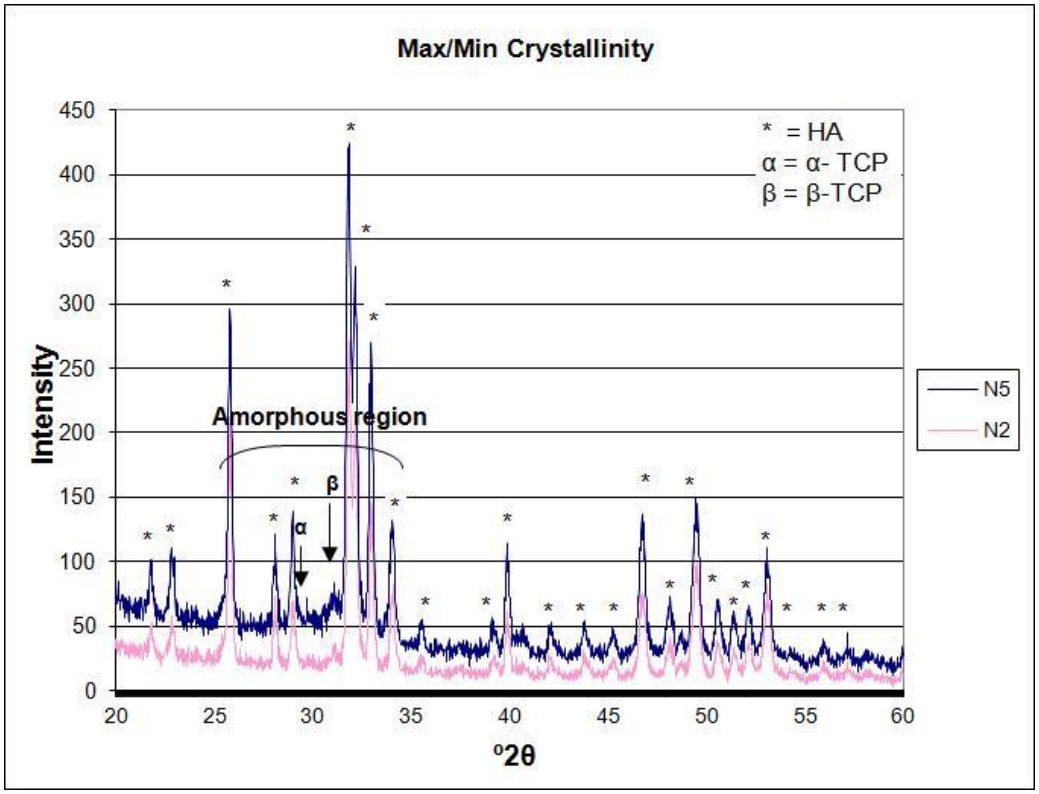

Figure 4: XRD patterns for samples with lowest (N5) and highest (N2) crystallinity. Graph shows the amorphous region and HA peaks (*), α-TCP peaks (α) and β-TCP peaks (β).

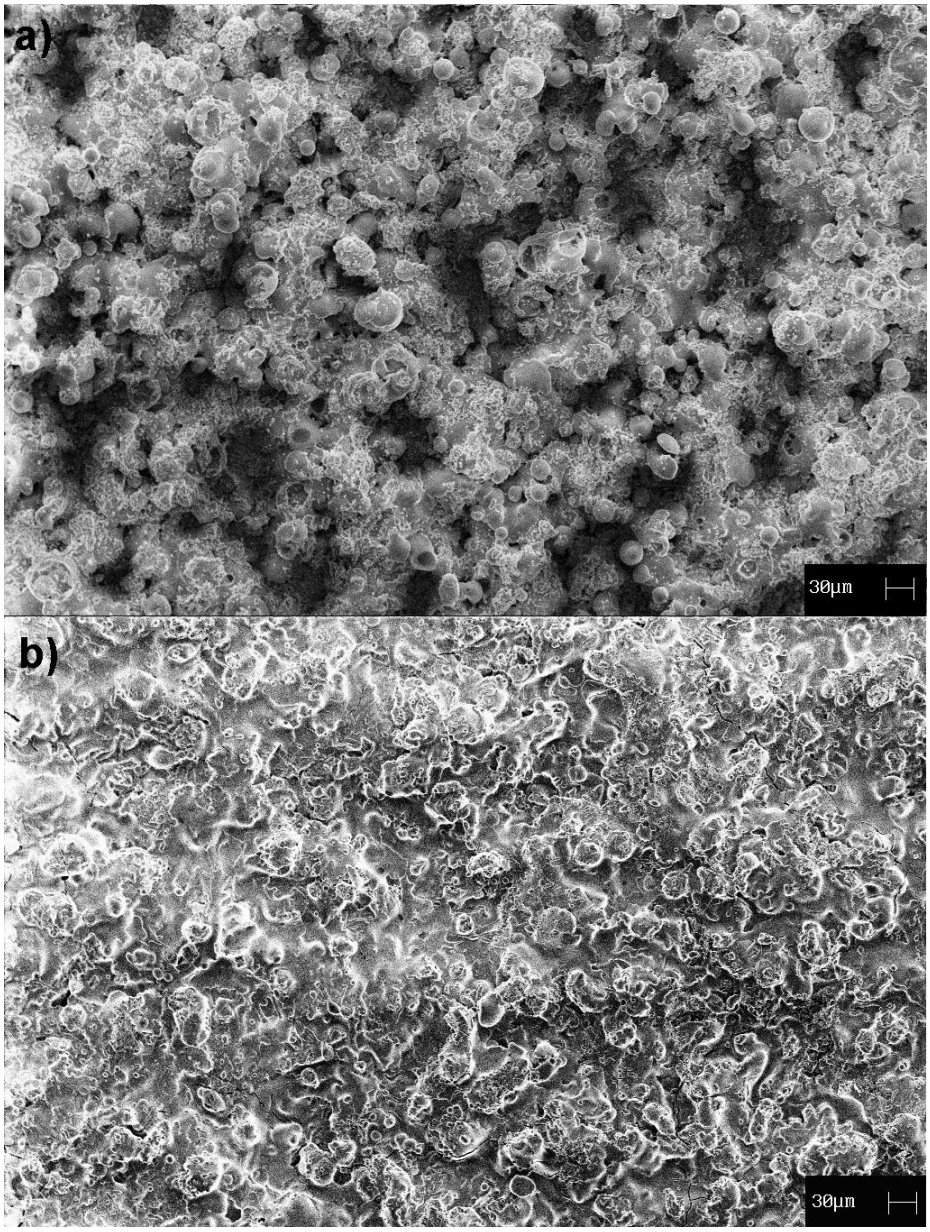

Figure 5: SEM micrographs showing surface morphology of a) Coating N5 and b) N2.

Coating N5 had the lowest crystallinity and coating N2 had the highest crystallinity.

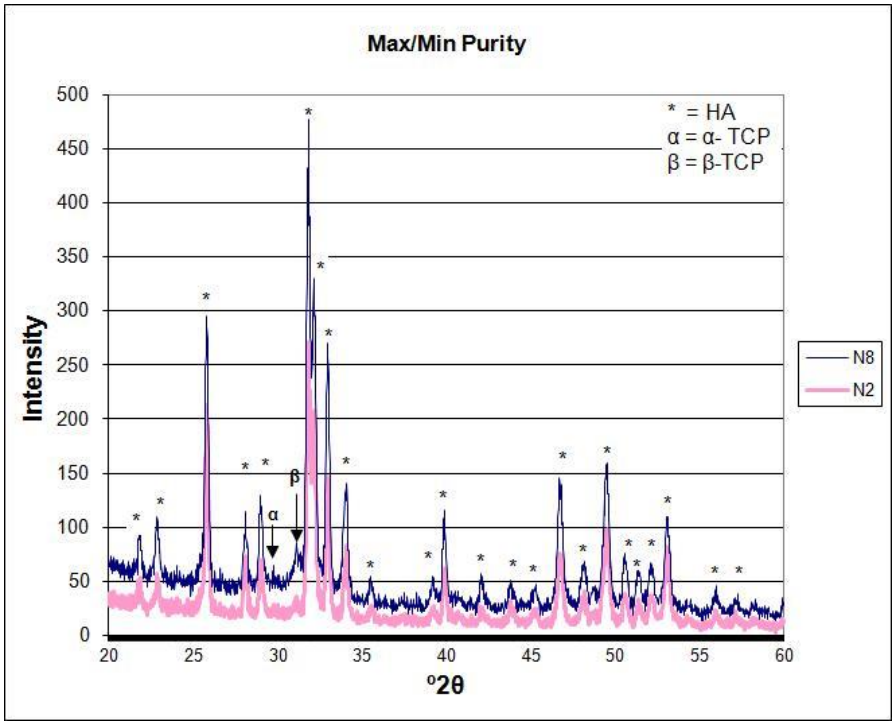

564

565 Figure 6: XRD patterns for samples with lowest (N8) and highest (N2) purity. Graph shows

566 HA peaks (*), α-TCP peaks (α) and β-TCP peaks (β).

567

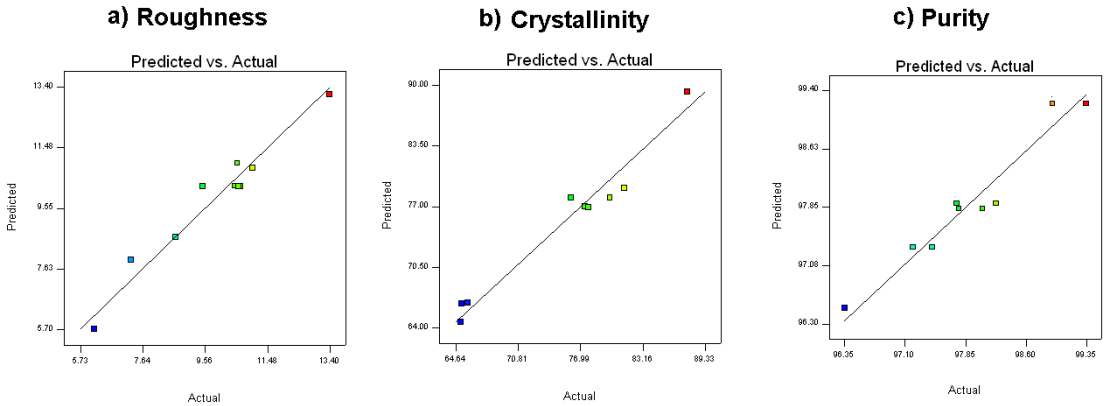

568

569 Figure 7: Predicted vs. Actual Plot for a) Roughness b) Crystallinity c) Purity. Graphs show

570 the relationship between the developed equation and actual experimental results.